IEEE Access
Multidisciplinary | Rapid Review | Open Access Journal

Received September 9, 2018, accepted October 2, 2018, date of publication October 24, 2018, date of current version August 26, 2019.

Digital Object Identifier 10.1109/ACCESS.2018.2875030

Robust Control of Grid-Tied Parallel Inverters Using Nonlinear Backstepping Approach

AMMAR AHMAD[1], NASIM ULLAH[2], NISAR AHMED[1], ASIER IBEAS[3], GHULAM MEHDI[4], JORGE HERRERA[5], AND ANWAR ALI[2]

[1]Faculty of Electronics Engineering, GIK Institute of Engineering Sciences and Technology, Topi 23460, Pakistan
[2]Department of Electronics Engineering, University of Technology, Nowshehra 24110, Pakistan
[3]Escola d'Enginyeria, Autonomous University of Barcelona, 08193 Barcelona, Spain
[4]Center of Excellence in Science and Applied Technology, Islamabad 44000, Pakistan
[5]Departamento de Ingeniería, Universidad de Bogotá Jorge Tadeo Lozano, Bogotá 110311, Colombia

Corresponding author: Asier Ibeas (asier.ibeas@uab.cat)

The work of A. Ibeas was supported in part by the Spanish Ministry of Economy and Competitiveness under Grant DPI2016-77271-R and in part by the University of Basque Country (UPV/EHU) under Grant PPG17/33.

ABSTRACT In modern electrical systems, solar energy extracted is integrated into electrical grid using power converters. In most cases, several inverters are connected across the same dc link so that the circulating currents between the inverter are made zero and the input power is shared among the available inverters. Because of the nonlinear nature of grid-tied photovoltaic (PV) system and the inherent modeling uncertainties, conventional control schemes cannot provide satisfactory performances under all operating conditions. Nonlinear control techniques for grid-tied inverter have been explored in this paper. However, the design of nonlinear controllers for the control of grid-tied parallel inverters has been rarely reported. Therefore, the purpose of this paper is to design a nonlinear controller for the control of grid-tied parallel inverter system. A novel control strategy is devised that utilizes backstepping inspired integral sliding mode control to maintain a constant dc link voltage and control power flow to the grid. An algorithm is developed, which determines the number of inverters connected across the dc link. The control strategy employs Lyapunov approach to ensure stability in an event of disturbance and guarantees robustness. With the proposed control scheme, better and superior performance is observed in transient response, total harmonic distortion minimization and integrating power into the grid at unity power factor. Furthermore, with the control strategy, the available power from the PV array is successfully distributed among multiple inverters operating in parallel.

INDEX TERMS Backstepping, dc link, ISMC, parallel inverters.

I. INTRODUCTION

In a grid-tied renewable energy system, power converters are used to transfer the DC power extracted from the PV array into AC power and integrate into the grid. Modern PV systems have the capability of generating power in several hundred megawatts. For such systems, it is desirable to divide the available input power among parallel inverters. Such an arrangement has a number of advantages over a system that employs a single inverter, e.g., it does not suffer from single point failure and has lower initial and maintenance costs [1]–[3]. For grid-tied inverters, the important control objectives are to keep the voltage and the frequency synchronized with the grid, control active and reactive flow to the grid and keep harmonic distortion below a standard limit [4]. For parallel operation of inverters, it is necessary to minimize the circulating currents among inverters [5]. For inverters connected across a common DC link capacitor, the circulating currents are no longer a problem as each inverter unit produces the same pulse width modulated (PWM) output [6].

The control of parallel inverter system has been carried out extensively in various studies [1], [7]–[18]. Control techniques employed in the literature are concentrated control [7], master-slave control [1], [8] and droop control [9]. Droop control is widely adopted because this control scheme does not require a communication line and truly forms a distributed system. In this control scheme, control is designed such that each inverter unit behaves as a synchronous machine, whose output voltage and frequency become a function of the active and reactive power drawn from it. The problems with this control scheme are slow tracking response, poor harmonic

handling when feeding nonlinear loads and the inability of the controller to provide balanced power sharing when operating under impedance mismatches of the line. In [11], a virtual impedance based droop control is proposed for balanced power sharing among inverters. The idea is to use a virtual impedance loop that dominates the impedance of the line. Although, balanced power sharing among various inverters is achieved, the power sharing is still poor. Meng *et al.* [12] proposed a generalized droop control (GDC) that derives from both the conventional droop and the virtual synchronous generator (VSG) controls. Using GDC, satisfactory performance is achieved in both grid connected and islanded modes of operation of the inverters. In [13], the conventional droop is modified such that active and reactive power are controlled considering a more general and realistic case of a system with complex impedance. This control strategy is more generic and is shown to control active and reactive power among several inverter units in case of resistive, inductive and complex impedances with a good transient response. Recently, a universal droop controller (UDC) is proposed in [14]. With UDC, the complete system is shown to be stable for impedance angle variation in the range $\theta \in (-\pi/2, \pi/2)$. Similarly, other modified forms of the droop control such as adaptive droop control [15]–[17] and robust droop control [18] have also been presented. These techniques give better power sharing with increased system stability.

Control techniques employing droop based control changes the output voltage and frequency depending upon the active and reactive power demands. In an AC grid, the frequency and voltage are predetermined and must remain constant. Therefore, in addition to the droop control, arrangements for the restoration of frequency and voltage amplitude have to be made once the system is loaded. Furthermore, synchronization schemes for voltage and frequency must also be incorporated in the control before making connection with the electrical grid. In [19]–[21], two additional control loops known as secondary and tertiary control loops have been proposed. Secondary control is used to restore the frequency and voltage amplitude while tertiary control is used for synchronization with the grid. The proposed control loops successfully restore the frequency and voltage as well as synchronize the PIS with the grid. However, it increases the complexity of the system and introduces a communication line between various stages of the control. Furthermore, because of the delays introduced in each stage, system might become unstable [22].

Control strategies designed on droop control use linear regulators to achieve control. A grid-tied PV system is a nonlinear system with inherent uncertainties. Linear control methods cannot guarantee stability under all operating conditions. Based on H_∞, the control of output current of inverter while taking into account the uncertain grid's impedance is reported in [23]. Khajehoddin *et al.* [24] have applied feedback linearization (FBL) to the control of grid-tied inverter. The nonlinear model of the system is translated into an equivalent linear model. Decoupling of active and reactive power is carried out using the *dq* transformation and PI controllers are used to track the direct and quadrature current components. Exploiting Lyapunov's theory, a robust nonlinear control scheme using partial feedback linearization is devised in [25]. Similarly, in [26], a nonlinear controller is designed in *abc* frame to control active and reactive power in a microgrid. Using direct power control (DPC), a sliding mode controller (SMC) is designed to track the references for active and reactive powers [27]. The control is carried out in $\alpha\beta$ reference frame so that information about the grid's angle is omitted. The controller is able to track active and reactive power and has a fast transient response. However, the scheme does not take into account the DC link dynamics. Benchagra *et al.* [28] have presented a nonlinear backstepping approach to control DC link voltage and power flow to the grid. Although, DC link voltage is controlled, there appear large oscillations in the output power. Similarly, in [29], a control scheme based on feedforward approach is devised. The controller gives a satisfactory transient response and minimizes the harmonics injected into the grid. An adaptive nonlinear control scheme based on backstepping approach is proposed in [30]. The design is verified to inject all the available power into the grid while controlling DC link voltage for step changes in the filter's inductance and DC link capacitance. Similarly in [31], another adaptive backstepping controller is designed for the control of grid-tied inverter. The controller is able to regulate active and reactive power flow to the grid. However, large oscillations still exist in the active and reactive powers. Furthermore, as the number of inverters connected to the system are increased, harmonics in the output current increase significantly.

In this paper, a novel control scheme for the control of grid-tied PIS using backstepping approach is devised. This paper considers the two stage grid-tied PV system in which the first stage deals with maximum power point tracking (MPPT). In this way, the power extracted from the PV array becomes independent of the level of DC link voltage. The three-phase model of the grid-tied PIS is converted into a rotating two phase system using *dq* transformation. The idea is to decouple active and reactive powers. A virtual control signal is used to control DC link voltage, whereas the actual control signals are used for tracking the direct and quadrature components of the current. The novelty of the paper lies in the fact that a backstepping inspired ISMC is designed for the control of grid-tied PIS. To the best knowledge of the authors, nonlinear controller using backstepping approach has not been designed for the control of grid-tied PIS.

This paper is organized as follows. Section II introduces the grid-tied PIS and details its modeling in *dq* reference frame. Control objectives and complete derivation of control laws based on Lyapunov's theory are given in section III. An algorithm that determines the number of inverters connected across the DC link is also developed in this section. Section IV shows validity of the control laws in achieving the control objectives in a simulation environment. Finally, conclusions are drawn in section V.

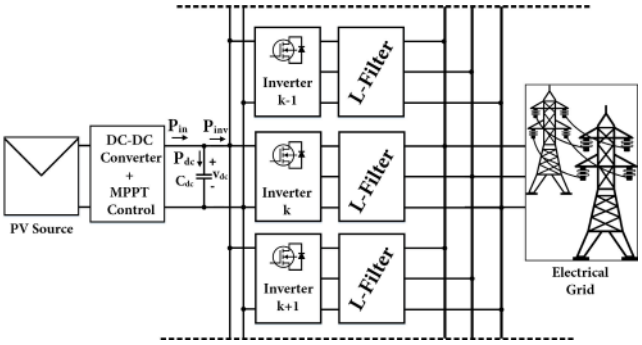

FIGURE 1. A grid-tied parallel inverter system fed by a PV source and connected across a common DC link capacitor.

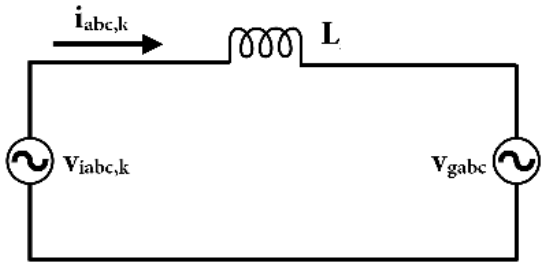

FIGURE 2. Simplified circuit diagram of the kth grid-tied inverter.

II. GRID-TIED PIS MODEL AND CONTROL OBJECTIVES

A. MODELLING OF GRID-TIED PIS

Fig. 1 shows a typical two stage grid-tied PIS. It is worth mentioning that the dotted lines in Fig. 1 indicate that, besides the three shown inverter units, the system can have many more inverter units. As mentioned in the previous section, such an arrangement decouples the power extracted from the PV array and DC link voltage. We assume that there are no switching losses in the power converters. Therefore, whatever power is extracted from the PV array, is readily available at the input of capacitor. This power is called input power or P_{in}. Each inverter is then connected to the grid through an L-filter. The purpose of the filter is to attenuate the harmonics generated as a result of switching phenomenon inside the inverters. Fig. 2 shows a simplified circuit diagram of the kth grid-tied inverter. Application of KVL to Fig. 2 leads to

$$\dot{i}_{a,k} = \frac{1}{L}\left(v_{ia,k} - v_{ga}\right) \tag{1a}$$

$$\dot{i}_{b,k} = \frac{1}{L}\left(v_{ib,k} - v_{gb}\right) \tag{1b}$$

$$\dot{i}_{c,k} = \frac{1}{L}\left(v_{ic,k} - v_{gc}\right) \tag{1c}$$

Here, $i_{abc,k}$, L, v_{gabc} and $v_{iabc,k}$ represent the currents fed into grid, filter's inductance, grid's voltage and inverter's output voltage respectively. The three phase system represented by (1a) through (1c) can be converted into dq frame as follows. First $abc-\alpha\beta$ transformation is obtained by applying Clarke's transformation matrix

$$\begin{bmatrix} v_\alpha \\ v_\beta \end{bmatrix} = \frac{2}{3}\begin{bmatrix} 1 & -1/2 & -1/2 \\ 0 & \sqrt{3}/2 & -\sqrt{3}/2 \end{bmatrix}\begin{bmatrix} v_a \\ v_b \\ v_c \end{bmatrix} \tag{2}$$

Using $\alpha\beta-dq$ transformation matrix, the stationary two phase quantities are transformed into synchronously rotating two phase DC quantities that rotates with angular velocity ω.

$$\begin{bmatrix} v_d \\ v_q \end{bmatrix} = \begin{bmatrix} \cos\theta & \sin\theta \\ -\sin\theta & \cos\theta \end{bmatrix}\begin{bmatrix} v_\alpha \\ v_\beta \end{bmatrix} \tag{3}$$

The final equations in dq frame are given by

$$\dot{i}_{d,k} = \omega i_{q,k} + \frac{1}{L}(v_{id,k} - v_{gd}) \tag{4a}$$

$$\dot{i}_{q,k} = -\omega i_{d,k} + \frac{v_{iq,k}}{L} \tag{4b}$$

The subscript k in (4a) and (4b) represents the parameters related to kth-inverter. Similarly the subscripts d and q represent the direct and quadrature components of the two phase quantities. It should be noted here that when the grid's angle $\theta = \omega t$ is used as a reference for dq transformation, the value of v_{gq} becomes zero. Referring to Fig. 1, the power equation can be written as

$$P_{dc} = P_{in} - \sum_{k=1}^{n} P_k \tag{5}$$

and

$$P_{dc} = C_{dc} v_{dc} \dot{v}_{dc} \tag{6}$$

Using the assumption that no switching losses occur in the inverter, the power absorbed by each inverter, represented by P_k, equals the power it feeds to the grid. Thus for dq frame, the relation for the output power of the inverter is given by (7)

$$P_k = \frac{3}{2} v_{gd} i_{d,k} \tag{7}$$

Using (6) and (7), (5) is re-written as

$$\dot{v}_{dc} = \frac{1}{C_{dc} v_{dc}}\left[P_{in} - \frac{3}{2}\left(v_{gd}\sum_{k=1}^{n} i_{d,k}\right)\right]$$

or

$$\dot{v}_{dc} = \frac{1}{C_{dc} v_{dc}}\left[P_{in} - \frac{3}{2} n v_{gd} i_{d,k}\right] \tag{8}$$

(4a), (4b) and (8) give the state-space model of the three-phase grid-tied PIS.

B. CONTROL OBJECTIVES

Following are the main control objectives of this paper.

1) Maintain a constant DC link voltage i.e. $v_{dc} = v_{dc}^*$.
2) Transfer all the available DC power into AC and integrate into electrical grid.
3) Keep a unity power factor.
4) Minimize THD.
5) Share the available power among various inverter units.

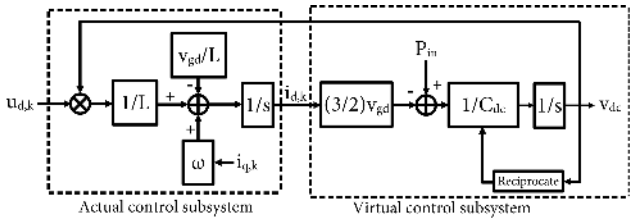

FIGURE 3. Cascaded structure used for backstepping control.

III. BACKSTEPPING ISMC CONTROLLER DESIGN

A. VIRTUAL CONTROL LAW

The two step cascade arrangement of the grid-tied PV system shown in Fig. 3 allows the exercise of backstepping control techniques to its control. The first subsystem has been named as the actual control subsystem since the actual control signal is the input to this block, whereas the succeeding subsystem is called the virtual control subsystem as the direct component of the current $i_{d,k}$ is its input and DC link voltage is its output. $i_{d,k}$ can be used as a virtual control signal to control the magnitude of the DC link voltage. Let v_{dc}^* be the reference DC link voltage and let $\vartheta_{dc} = v_{dc}^* - v_{dc}$ be the corresponding tracking error. Let $i_{d,k}^*$ be the virtual control signal that drives v_{dc} upon v_{dc}^*. With ISMC, the integral of the error becomes a variable of interest which raises the relative degree by 1 [32]. Therefore, the sliding manifold for the error in DC link voltage becomes

$$\Psi_{dc} = \vartheta_{dc} + \xi_{dc} \int \vartheta_{dc} dt \tag{9}$$

where $\xi_{dc} > 0$. The time derivative of (9) yields

$$\dot{\Psi}_{dc} = \frac{1}{C_{dc} v_{dc}} \left(\frac{3}{2} n v_{gd} i_{d,k} - P_{in} \right) + \xi_{dc} (v_{dc}^* - v_{dc}) \tag{10}$$

By setting (10) equal to zero, it is observed that $\dot{\vartheta}_{dc} = -\xi_{dc} \vartheta_{dc}$ which represents the first order asymptotically stable dynamics. The virtual control signal $i_{d,k}^*$ is then written as

$$i_{d,k}^* = \frac{2P_{in}}{3nv_{gd}} - \frac{2C_{dc} v_{dc} \xi_{dc}}{3nv_{gd}} (v_{dc}^* - v_{dc}) \tag{11}$$

B. ACTUAL CONTROL LAWS

The active power flow to the grid is regulated by enforcing $i_{d,k}$ to follow the trajectory of $i_{d,k}^*$. This reference current is dictated by (11) which in itself is domineered by the power extracted from the PV array. Similarly, the reactive power is dominated only by the quadrature component of the current $i_{q,k}$. The reference for this current $i_{q,k}^* = \frac{-2Q_k^*}{3v_{gd}}$ is kept zero to ensure power feeding at unity power factor. The tracking errors in the direct and quadrature currents are given by (12a) and (12b) respectively

$$\vartheta_{d,k} = i_{d,k}^* - i_{d,k} \tag{12a}$$
$$\vartheta_{q,k} = i_{q,k}^* - i_{q,k} \tag{12b}$$

Consider the derivative of $i_{d,k}^*$

$$\dot{i}_{d,k}^* = \frac{d}{dt} \left[\frac{2P_{in}}{3nv_{gd}} - \frac{2C_{dc} v_{dc} \xi_{dc}}{3nv_{gd}} (v_{dc}^* - v_{dc}) \right] \tag{13}$$

Because v_{gd} remains necessarily constant, therefore

$$\dot{i}_{d,k}^* = \frac{2\dot{P}_{in}}{3nv_{gd}} - \frac{d}{dt} \left[\frac{2C_{dc} v_{dc} \xi_{dc}}{3nv_{gd}} (v_{dc}^* - v_{dc}) \right]$$

or

$$\dot{i}_{d,k}^* = \frac{2\dot{P}_{in}}{3nv_{gd}} - \frac{2C_{dc} \dot{v}_{dc} \xi_{dc}}{3nv_{gd}} (v_{dc}^* - 2v_{dc}) \tag{14}$$

where $\dot{P}_{in}$ and $\dot{v}_{dc}$ represent the derivatives of P_{in} and v_{dc} respectively. The sliding trajectories for the direct and quadrature currents are defined as

$$\Psi_{d,k} = \vartheta_{d,k} + \xi_{gd} \int \vartheta_{d,k} dt \tag{15a}$$
$$\Psi_{q,k} = \vartheta_{q,k} + \xi_{gq} \int \vartheta_{q,k} dt \tag{15b}$$

where ξ_{gd} and ξ_{gq} are both greater than zero. Taking derivative of (15a) and (15b) gives

$$\dot{\Psi}_{d,k} = \dot{\vartheta}_{d,k} + \xi_{gd} \vartheta_{d,k} \tag{16a}$$
$$\dot{\Psi}_{q,k} = \dot{\vartheta}_{q,k} + \xi_{gq} \vartheta_{q,k} \tag{16b}$$

Also using (4a) and (11), the following are obtained

$$\dot{\vartheta}_{d,k} = \frac{2\dot{P}_{in}}{3nv_{gd}} - \frac{2C_{dc} \dot{v}_{dc} \xi_{dc}}{3nv_{gd}} (v_{dc}^* - 2v_{dc}) - \omega i_{q,k} - \frac{1}{L} (v_{id,k} - v_{gd}) \tag{17}$$
$$\dot{\vartheta}_{q,k} = \omega i_{d,k} - \frac{v_{iq,k}}{L} \tag{18}$$

In order to obtain the actual control laws, the candidate Lyapunov energy-like functions are defined as

$$\Phi_{d,k} = \frac{1}{2} \Psi_{d,k}^2 > 0 \tag{19a}$$
$$\Phi_{q,k} = \frac{1}{2} \Psi_{q,k}^2 > 0 \tag{19b}$$

For asymptotic stability, the derivative of (19a) and (19b) must always be negative, thus

$$\dot{\Phi}_{d,k} = \Psi_{d,k} \dot{\Psi}_{d,k} < 0 \tag{20a}$$
$$\dot{\Phi}_{q,k} = \Psi_{q,k} \dot{\Psi}_{q,k} < 0 \tag{20b}$$

Realizing that the two phase output voltages of each inverter are the product of v_{dc} and the corresponding switching signal (control signal) i.e. $v_{id,k} = u_{d,k} v_{dc}$, $v_{iq,k} = u_{q,k} v_{dc}$, (16a) and (16b) are re-written as

$$\dot{\Psi}_{d,k} = \dot{i}_{d,k}^* - \left[\omega i_{q,k} + \frac{1}{L} (u_{d,k} v_{dc} - v_{gd}) \right] + \xi_{gd} (i_{d,k}^* - i_{d,k}) \tag{21}$$
$$\dot{\Psi}_{q,k} = \omega i_{d,k} - \frac{1}{L} u_{q,k} v_{dc} + \xi_{gq} (i_{q,k}^* - i_{q,k}) \tag{22}$$

Now the equivalent control laws, represented mathematically by $u_{deq,k}$ and $u_{qeq,k}$ enforce the system to follow the desired trajectories $\Psi_{d,k} = 0$ and $\Psi_{q,k} = 0$ and are given by

$$u_{deq,k} = \frac{L}{v_{dc}}\left[\frac{v_{gd}}{L} - \omega i_{q,k} + \dot{i}^*_{d,k} + \xi_{gd}(i^*_{d,k} - i_{d,k})\right]$$

and

$$u_{qeq,k} = \frac{L}{v_{dc}}\left[\omega i_{d,k} + \xi_{gq}(i^*_{q,k} - i_{q,k})\right]$$

or

$$u_{deq,k} = \frac{L}{v_{dc}}\left[\frac{v_{gd}}{L} - \omega i_{q,k} - \frac{2C_{dc}\dot{v}_{dc}\xi_{dc}}{3nv_{gd}}(v^*_{dc} - 2v_{dc}) + \frac{2\dot{P}_{in}}{3nv_{gd}} + \xi_{gd}(i^*_{d,k} - i_{d,k})\right] \quad (23)$$

and

$$u_{qeq,k} = \frac{L}{v_{dc}}\left[\omega i_{d,k} + \xi_{gq}(i^*_{q,k} - i_{q,k})\right] \quad (24)$$

C. ROBUSTNESS OF CONTROL LAWS

The equivalent control laws guarantee stable tracking of the system's trajectories. However, the steady state tracking performance might get affected in an event of disturbance. To achieve tracking even in the presence of disturbance, the equivalent control laws (23) and (24) are modified by adding discontinuous signum terms $sign(\Psi_{d,k})$ and $sign(\Psi_{q,k})$ such that the net control laws take the form

$$u_{d,k} = \frac{L}{v_{dc}}\left[-\omega i_{q,k} + \frac{2\dot{P}_{in}}{3nv_{gd}} - \frac{2C_{dc}\dot{v}_{dc}\xi_{dc}}{3nv_{gd}}(v^*_{dc} - 2v_{dc}) + \frac{v_{gd}}{L} + \xi_{gd}(i^*_{d,k} - i_{d,k})\right] - \zeta_{d,k}sign(\Psi_{d,k}) \quad (25)$$

$$u_{q,k} = \frac{L}{v_{dc}}\left[\omega i_{d,k} + \xi_{gq}(i^*_{q,k} - i_{q,k})\right] - \zeta_{q,k}sign(\Psi_{q,k}) \quad (26)$$

where $\zeta_{d,k}$ and $\zeta_{q,k}$ are some positive constants.

D. PROOF OF ROBUSTNESS

Let the maximum of disturbances in the system dynamics defined by (4a) and (4b) be represented by $\Upsilon_{d,k}$ and $\Upsilon_{q,k}$ respectively, then after incorporating the disturbance terms and substituting (25) and (26) into (20a) and (20b) respectively, we obtain

$$\Psi_{d,k}\dot{\Psi}_{d,k} = \Psi_{d,k}\Upsilon_{d,k} - \zeta_{d,k}\Psi_{d,k}sign(\Psi_{d,k})$$
$$\Psi_{q,k}\dot{\Psi}_{q,k} = \Psi_{q,k}\Upsilon_{q,k} - \zeta_{q,k}\Psi_{q,k}sign(\Psi_{q,k})$$

or

$$\Psi_{d,k}\dot{\Psi}_{d,k} = \Psi_{d,k}\Upsilon_{d,k} - \zeta_{d,k}|\Psi_{d,k}| \quad (27)$$
$$\Psi_{q,k}\dot{\Psi}_{q,k} = \Psi_{q,k}\Upsilon_{q,k} - \zeta_{q,k}|\Psi_{q,k}| \quad (28)$$

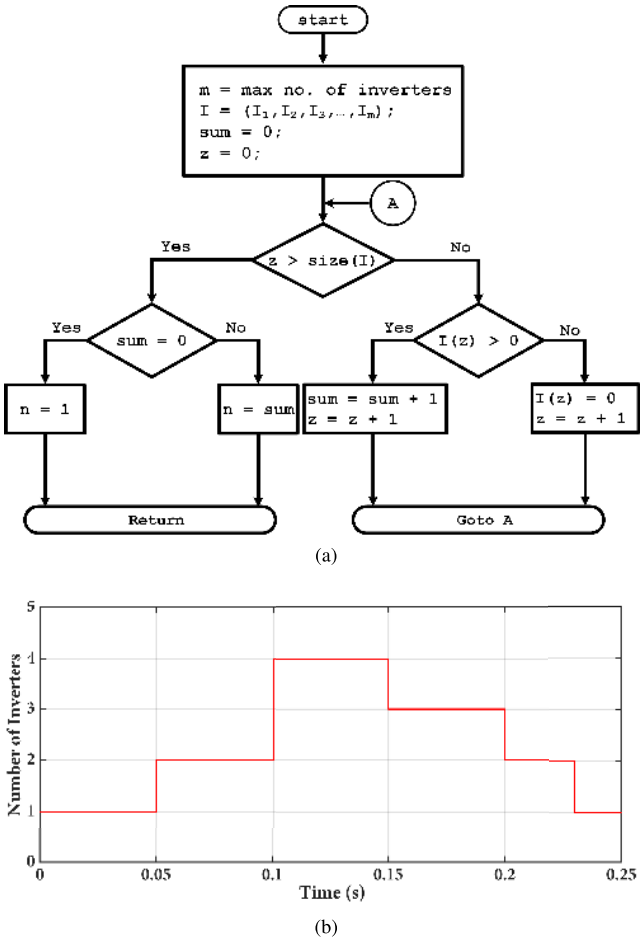

FIGURE 4. (a). Algorithm for determining the number of inverters connected across the DC link. (b). Simulation results.

For $\Psi_{d,k} < 0$ and $\Psi_{q,k} < 0$, both (27) and (28) are less than zero and hence asymptotic stability is ensured. However, for $\Psi_{d,k} > 0$ and $\Psi_{q,k} > 0$, asymptotic stability is realized only when the constants $\zeta_{d,k}$ and $\zeta_{q,k}$ are chosen such that

$$\zeta_{d,k} > \Upsilon_{d,k} \quad (29a)$$
$$\zeta_{q,k} > \Upsilon_{q,k} \quad (29b)$$

The gains of the ISMC controller can be tuned using a technique detailed in [33]. Newton's optimization technique is used to compute the optimal gains that minimize the tracking errors. The gains of the ISMC controller $\zeta_{d,k}$ and $\zeta_{q,k}$ are initialized to values defined by (29a) and (29b) respectively before running the iterations for gain tuning. Furthermore, since the tuning technique provides the gains that minimize the error, we can safely deduce that error will converge to zero asymptotically. It is also worth mentioning that because the gains are tuned according to the existing state of the error, robustness against disturbances is established once again. This is because the error on a particular state increases in the presence of disturbance. This increase in error can only be minimized if the gains are tuned to values defined by (29a) and (29b).

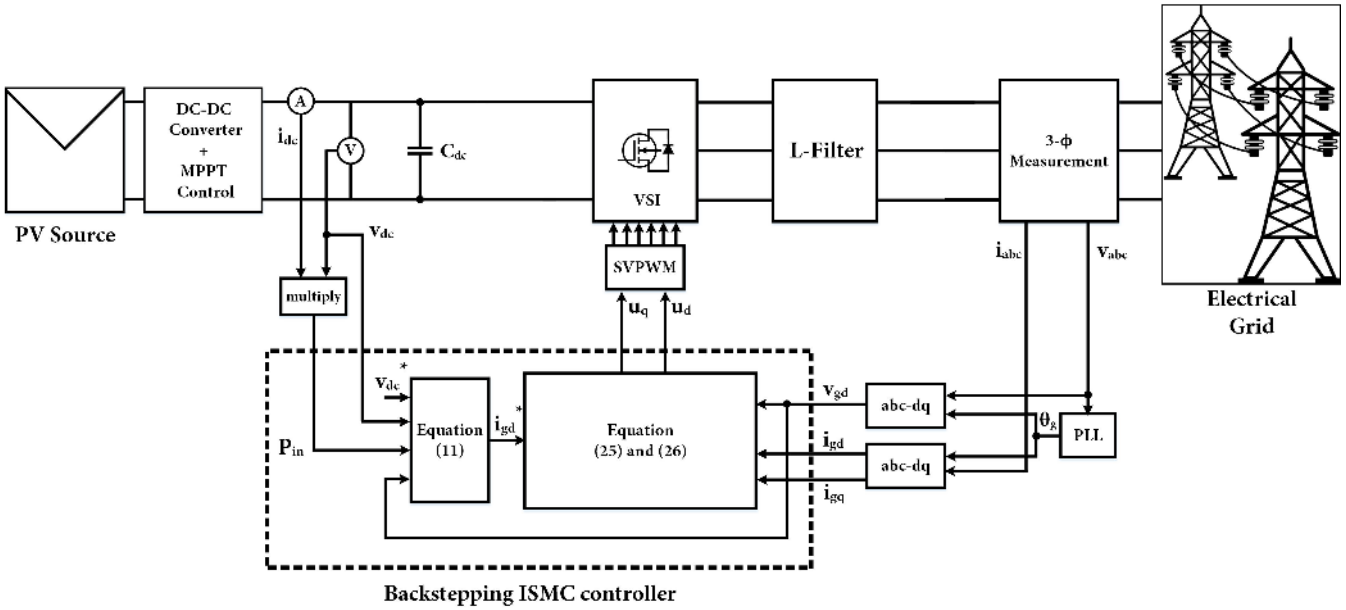

FIGURE 5. Implemented system with a single inverter unit.

E. MECHANISM FOR DETERMINING NUMBER OF CONNECTED INVERTERS

The reference current $i^*_{d,k}$ depends upon the number of inverters n, connected across the DC link. Therefore, determining this number while the system is up and running is of the utmost importance. A wrong reference value might lead to undesirable results. Let m be the maximum number of inverters connected across the DC link and let $I_1, I_2, I_3, ..., I_m$ be the currents of the corresponding inverter units. Disconnected inverters correspond to zero currents. This fact has been used to our advantage. Fig. 4a shows the algorithm developed to determine n. The algorithm reads in all the available currents from various inverter units (I_1 through I_m) and stores them in an array I (input current ports for disconnected inverters might be grounded to read zero). Two variables *sum* and z are defined and initialized to zero (z must be initialized to 1 if coding is to be carried out in Matlab). The algorithm searches the array and increments the variable *sum* each time it encounters a non zero entry. This process goes on until the variable z becomes greater than the size of the array. If no inverter unit is connected, the algorithm must output $n = 1$. This is done to avoid infinite values of the reference $i^*_{d,k}$. For the case, where $0 < n \leq m$, the algorithm outputs the number of connected inverters.

In order to verify the algorithm developed, four inverter units are used. Initially all the inverters are disconnected so that the algorithm outputs $n = 1$. At $t = 0.05$ s, two inverter units are connected. The algorithm now outputs $n = 2$. At $t = 0.1$ s, the remaining two inverters are also connected. The algorithm must now output $n = 4$. At $t = 0.15$ s and $t = 0.2$ s, the third and fourth inverter units are disconnected respectively. Finally, at $t = 0.23$ s, the first two inverters are also disconnected. The result of simulation shown in Fig. 4b verifies the algorithm.

F. SYSTEM IMPLEMENTATION

Fig. 5 shows a two stage control in which the first stage deals with extracting maximum power from the PV array. The second stage is associated with the control of power flow to the grid along with other control objectives given in section II-B. In order to achieve maximum power point tracking (MPPT), a SMC based MPPT controller is designed. However, for the sake of brevity its design is not included here. The backstepping control laws derived in (25) and (26) are used to pilot the SVPWM block that generates six switching signals. These switching signals or sequences are used to drive the six IGBTs of each inverter unit. Simulation of the complete system is carried out in Matlab Simulink (version R2017a) environment.

IV. SIMULATION RESULTS

The simulation for the control of grid-tied inverters is divided into two parts. In first part, a single inverter is connected across the DC link. In second part, multiple inverters are connected across the same DC link capacitor.

A. SINGLE INVERTER UNIT

A PV array capable of generating 10 kW at 1 kW m^{-2} and 25 °C is designed to supply the input power. Simulation results are given in Fig. 6. The initial voltage of the DC link capacitor as well as its voltage reference v^*_{dc} are both kept at 550 V. The reference for direct component of the current is governed by the amount of power available from the PV array. Initially P_{in} is zero, however, during time

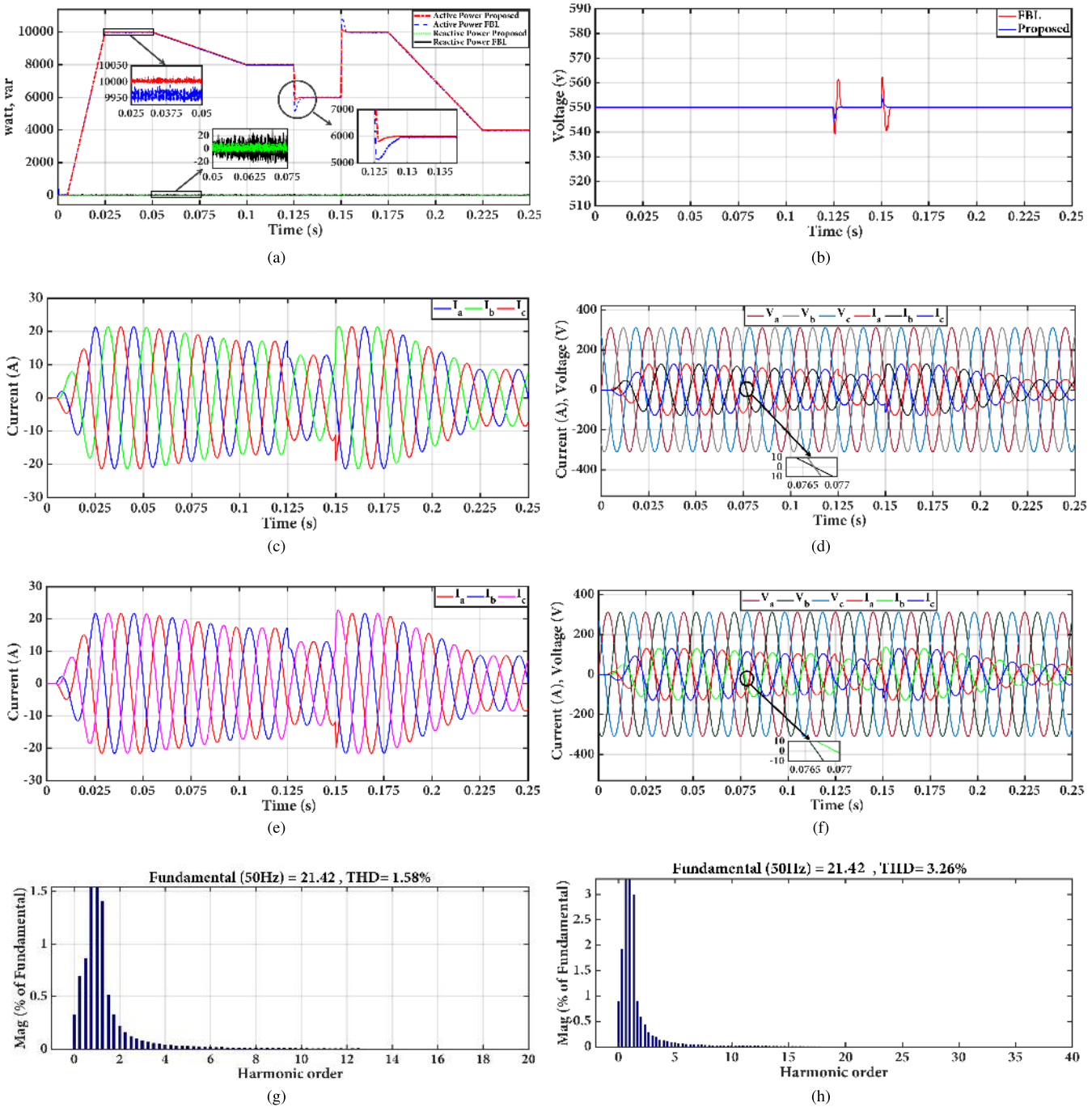

FIGURE 6. Simulation results for a single inverter unit. A comparison between the proposed controller and FBL controller. (a) Active and reactive power fed into the grid. (b). DC link voltage. (c). Three-phase currents of the proposed controller. (d). Power factor analysis of the proposed controller. For better viewing, three-phase currents are amplified six times. Corresponding voltage and current phases are in phase. (e). Three-phase currents of the FBL controller. (f). Power factor analysis of the FBL controller. Although reactive power is zero, because of the small tracking error and relatively slow tracking by the FBL controller, the power factor is not exactly 1. (g) THD in the output currents with the proposed controller and (h). THD in the output currents with FBL controller at 2.5 kW and 1 kvar.

$t = 0.0121$ s-0.025 s it rises linearly to 10 kW and thereafter remains constant. At $t = 0.05$ s, P_{in} suffers a ramp decay and becomes constant at 8 kW. At $t = 0.125$ s, it suffers another step decay to 6 kW and a step rise to 10 kW at $t = 0.15$ s. It then undergoes another ramp decay at $t = 0.175$ s to reach 4 kW at $t = 0.225$ s after which it remains constant till the end of simulation. The reference for reactive power is kept zero all the time to ensure power feeding at unity power factor. The circuit and control parameters for the proposed controller are summarized in Table 1. For the sake of comparison with

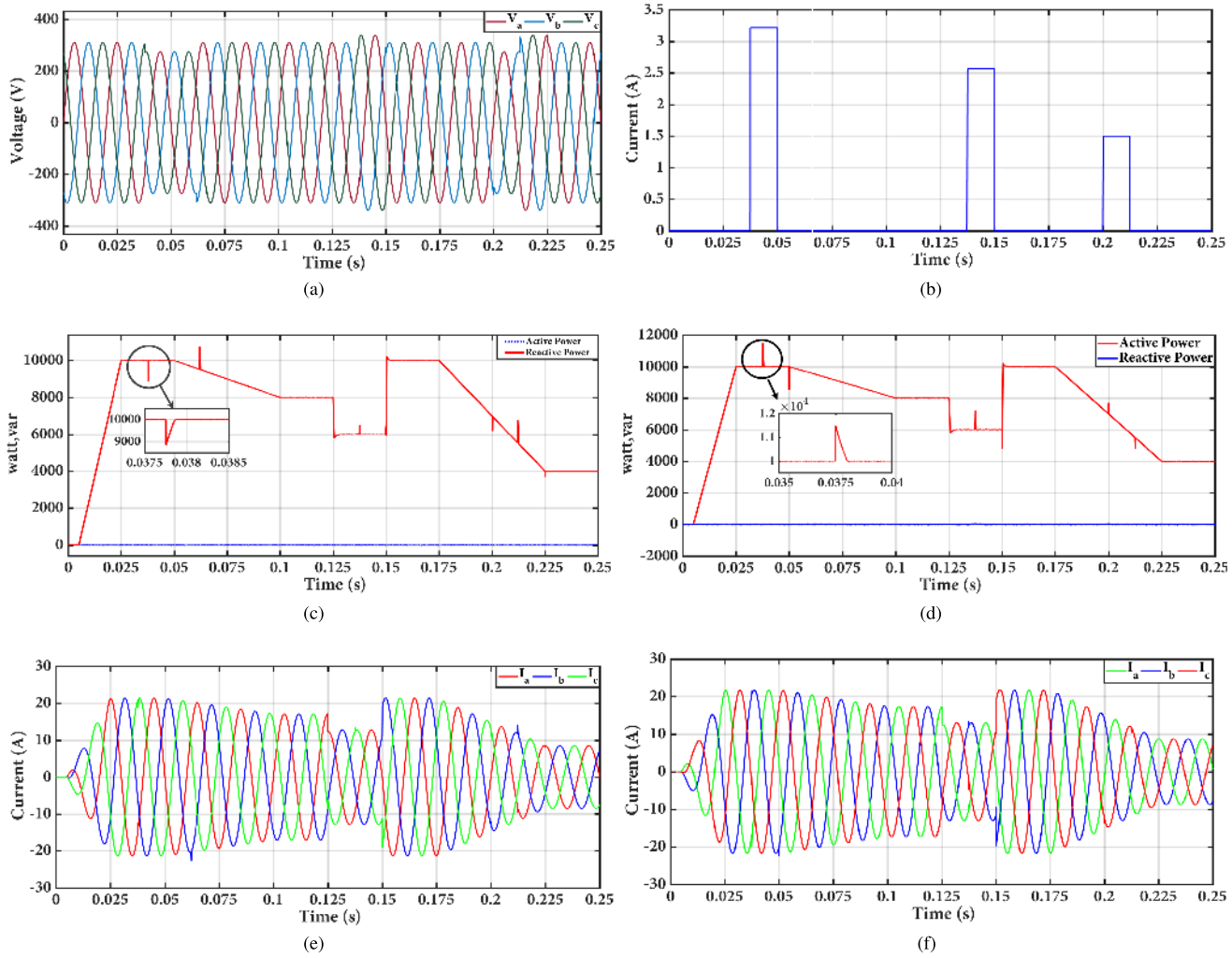

FIGURE 7. Simulation results showing the performance of the proposed controller in the presence of disturbances. (a). Disturbance in voltage of the grid in form of voltage dips and rises. (b). 15%, 20% and 10% of reference signal is injected as disturbance (c). Active and reactive power profile in response to voltage dips and rises. (d). Active and reactive power profile in response to disturbance shown in (b). (e). Three-phase currents in case of disturbance shown in (a). (f). Three-phase currents in case of disturbance shown in (b).

TABLE 1. System and control parameters.

Parameter	Value
DC link capacitor, C_{dc}	470 µF
Switching frequency, f_{sw}	10 kHz
Filter's Inductance, L	8 mH
Grid's voltage (RMS)	220 V
Grid's frequency, f	50 Hz
ξ_{dc}	3×10^4
ξ_{gd}	5×10^3
ξ_{gq}	1×10^3
$\zeta_{d,k}$	2×10^3
$\zeta_{q,k}$	3.5×10^3

the state-of-the-art control technique, the same scenario is simulated using both the proposed controller and the FBL controller [24]. Simulation results (see Fig. 6) establish the superior performance of the proposed controller in tracking reference signals, transient response and THD minimization. Furthermore, Fig. 6h shows that even though the reactive power reference is kept zero, power factor in case of FBL controller is not exactly 1. This might be the result of the relatively slow tracking of the FBL controller and the small tracking error. On the other hand, the proposed controller has done a better job at keeping a unity power factor.

B. DISTURBANCE REJECTION

Disturbance rejection capability of the proposed controller was proved in section III-D. In this section, a disturbance injection scenario is simulated to verify the reference tracking capability of the proposed controller in the presence of disturbance. According to [34], one of the common disturbances in an electrical grid is a voltage dip or sag. Specifically a voltage drop (amplitude between 90% and 10%) or a rise (amplitude between 110% and 180%) of the nominal voltage is observed.

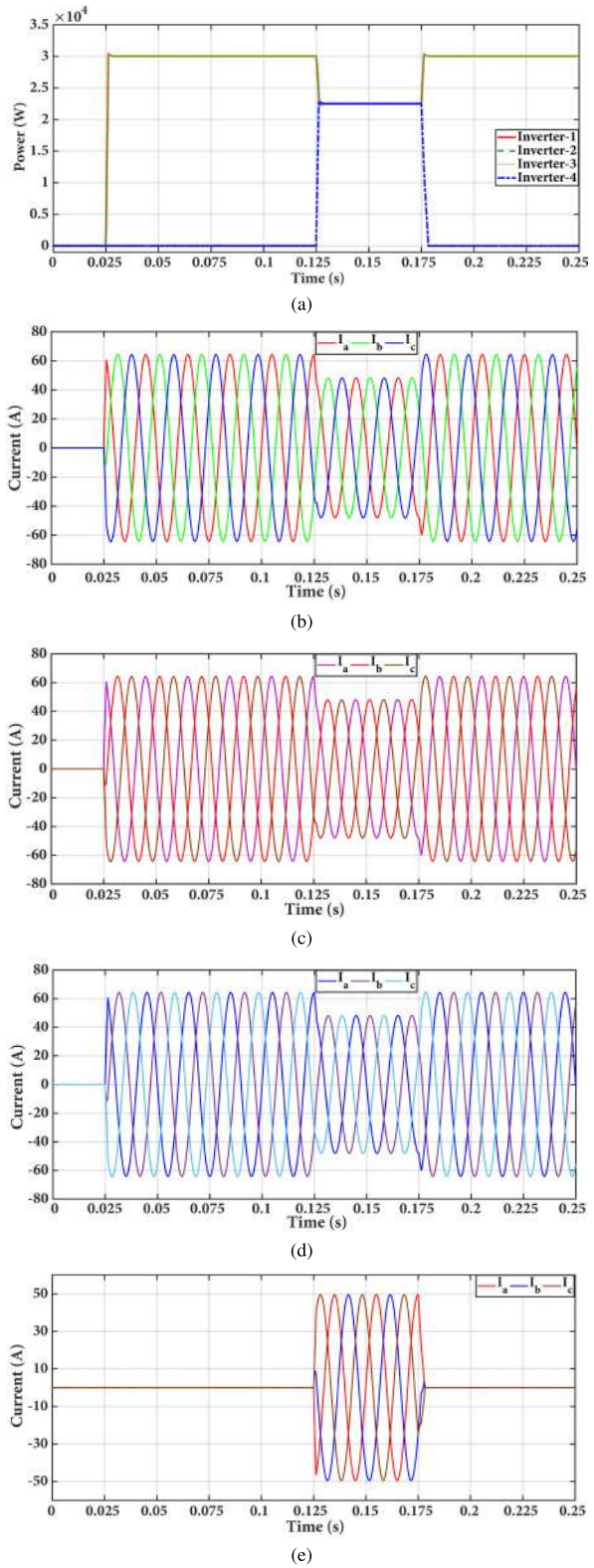

FIGURE 8. Simulation results for the multiple inverter units. (a). Power sharing among four inverters. Power per inverter changes whenever a unit is connected or disconnected. (b)-(d). Inverter-1 through inverter-4's currents.

Therefore, voltage variations in the nominal voltage of the grid is introduced at different times. Initially at $t = 0.03775$ s, a voltage dip ($v_{rms} = 10$ V) is commenced that lasts till $t = 0.0625$ s. Then at $t = 0.1375$ s, the voltage was increased to 10% above the nominal value and was restored at $t = 0.15$ s. Finally, another voltage dip is introduced at $t = 0.2$ s which is immediately followed by a rise at $t = 0.2125$ s. Simulation results of Fig. 7 depict that the proposed controller is able to track the current references despite the voltage dips and rises. As pointed out by one of the reviewer, one possible disturbance scenario would be to inject certain percentages of the reference signal at different times. Therefore, 15%, 20% and 10% of the reference signals are injected at $t = 0.03775$ s, $t = 0.1375$ s and $t = 0.2$ s respectively. Simulation results once again establish the disturbance rejection capability of the proposed controller.

C. MULTIPLE INVERTER UNITS

In this section, the ability of the controller (along with the developed algorithm) to share power among various inverters is verified. A PV array capable of generating 90 kW of power at standard conditions is used. The simulation is carried out using four inverters. The size of L filter is changed to 3 mH. Initially, no inverter is connected so that power delivered to the grid is zero. At $t = 0.025$ s, three inverters are connected. Of the total 90 kW, each inverter unit provides 33.3% or 30 kW. At the instant of 0.125 s, the fourth inverter is connected such that the power delivered by each inverter to the grid drops down to 25% or 22.5 kW. At $t = 0.175$ s the fourth inverter is disconnected and the power per inverter rises up again to 30 kW. The simulation results shown in Fig. 8 hence verify the effectiveness of controller in achieving objective 5.

V. CONCLUSION

In this paper, a nonlinear backstepping inspired ISMC controller is designed for the control of grid-tied PIS. The objectives of the research work are to 1) maintain a constant DC link voltage, 2) integrate the available power from the PV array into the grid at unity power factor and 3) minimize THD, 4) share available power among various inverters operating in parallel. Control scheme is designed such that the reference for active current component changes each time an inverter unit is connected to the system. An algorithm is also developed which determines the number of inverters connected across the DC link. Simulation results establish that the proposed controller has superior performance in transient response, THD minimization and power regulation as compared to the FBL controller. Furthermore, the proposed controller is robust and is able to track the desired trajectories despite the disturbances and the voltage dips on the line. It is shown that with the proposed control scheme, power is shared among multiple inverters operating in parallel. Close analysis of the simulation results for single inverter unit and multiple inverter units reveal that with an increase in the level of power, the L-filter size can be reduced significantly without violating THD limit.

ACKNOWLEDGMENT

A. Ahmad would like to thank the contribution of Dr. N. Ullah for providing invaluable technical support in completing the research work. Dr. N. Ullah would like to thank the Higher Education Commission (HEC) Pakistan, for providing the PCCR research grant to travel the Dr. Asier Ibeas Research Group, UAB, Barcelona, Spain, and the contribution of Dr. A. Ibeas for providing technical support during the short visit.

REFERENCES

[1] J.-F. Chen and C.-L. Chu, "Combination voltage-controlled and current-controlled PWM inverters for UPS parallel operation," *IEEE Trans. Power Electron.*, vol. 10, no. 5, pp. 547–558, Sep. 1995.

[2] T. F. Wu, H. M. Hsieh, Y. E. Wu, and Y. K. Chen, "Parallel-inverter system with failure isolation and hot-swap features," *IEEE Trans. Ind. Appl.*, vol. 43, no. 5, pp. 1329–1340, Sep. 2007.

[3] X. Yu and A. M. Khambadkone, "Reliability analysis and cost optimization of parallel-inverter system," *IEEE Trans. Ind. Electron.*, vol. 59, no. 10, pp. 3881–3889, Oct. 2012.

[4] F. Blaabjerg, R. Teodorescu, M. Liserre, and A. V. Timbus, "Overview of control and grid synchronization for distributed power generation systems," *IEEE Trans. Ind. Electron.*, vol. 53, no. 5, pp. 1398–1409, Oct. 2006.

[5] H. Cai, R. Zhao, and H. Yang, "Study on ideal operation status of parallel inverters," *IEEE Trans. Power Electron.*, vol. 23, no. 6, pp. 2964–2969, Nov. 2008.

[6] C. Song, R. Zhao, M. Zhu, and Z. Zeng, "Operation method for parallel inverter system with common DC link," *IET Power Electron.*, vol. 7, no. 5, pp. 1138–1147, 2013.

[7] M. C. Chandorkar, D. M. Divan, and R. Adapa, "Control of parallel connected inverters in standalone AC supply systems," *IEEE Trans. Ind. Appl.*, vol. 29, no. 1, pp. 136–143, Jan./Feb. 1993.

[8] J. Holtz and K.-H. Werner, "Multi-inverter UPS system with redundant load sharing control," *IEEE Trans. Ind. Electron.*, vol. 37, no. 6, pp. 506–513, Dec. 1990.

[9] M. Arias, D. Lamar, M. Rodriguez, M. Hernando, and A. Fernandez, "Simple droop voltage control system for parallel operation of UPS," in *Proc. 23rd Annu. IEEE Appl. Power Electron. Conf. Exposit. (APEC)*, Feb. 2008, pp. 1946–1951.

[10] N. Pogaku, M. Prodanovic, and T. C. Green, "Modeling, analysis and testing of autonomous operation of an inverter-based microgrid," *IEEE Trans. Power Electron.*, vol. 22, no. 2, pp. 613–625, Mar. 2007.

[11] J. M. Guerrero, L. Garcia de Vicuna, J. Matas, M. Castilla, and J. Miret, "Output impedance design of parallel-connected UPS inverters with wireless load-sharing control," *IEEE Trans. Ind. Electron.*, vol. 52, no. 4, pp. 1126–1135, Aug. 2005.

[12] X. Meng, J. Liu, and Z. Liu, "A generalized droop control for grid-supporting inverter based on comparison between traditional droop control and virtual synchronous generator control," *IEEE Trans. Power Electron.*, vol. 34, no. 6, pp. 5416–5438, Jun. 2019.

[13] W. Yao, M. Chen, J. Matas, J. M. Guerrero, and Z.-M. Qian, "Design and analysis of the droop control method for parallel inverters considering the impact of the complex impedance on the power sharing," *IEEE Trans. Ind. Electron.*, vol. 58, no. 2, pp. 576–588, Feb. 2011.

[14] Q.-C. Zhong and Y. Zeng, "Universal droop control of inverters with different types of output impedance," *IEEE Access*, vol. 4, pp. 702–712, 2016.

[15] M. B. Delghavi and A. Yazdani, "An adaptive feedforward compensation for stability enhancement in droop-controlled inverter-based microgrids," *IEEE Trans. Power Del.*, vol. 26, no. 3, pp. 1764–1773, Jul. 2011.

[16] J. Kim, J. M. Guerrero, P. Rodriguez, R. Teodorescu, and K. Nam, "Mode adaptive droop control with virtual output impedances for an inverter-based flexible AC microgrid," *IEEE Trans. Power Electron.*, vol. 26, no. 3, pp. 689–701, Mar. 2011.

[17] K. Yu, Q. Ai, S. Wang, J. Ni, and T. Lv, "Analysis and optimization of droop controller for microgrid system based on small-signal dynamic model," *IEEE Trans. Smart Grid*, vol. 7, no. 2, pp. 695–705, Mar. 2016.

[18] Q.-C. Zhong, "Robust droop controller for accurate proportional load sharing among inverters operated in parallel," *IEEE Trans. Ind. Electron.*, vol. 60, no. 4, pp. 1281–1290, Apr. 2013.

[19] J. C. Vasquez, J. M. Guerrero, J. Miret, M. Castilla, and L. G. De Vicuna, "Hierarchical control of intelligent microgrids," *IEEE Ind. Electron. Mag.*, vol. 4, no. 4, pp. 23–29, Dec. 2010.

[20] J. M. Guerrero, J. C. Vasquez, J. Matas, L. G. De Vicuña, and M. Castilla, "Hierarchical control of droop-controlled AC and DC microgrids—A general approach toward standardization," *IEEE Trans. Ind. Electron.*, vol. 58, no. 1, pp. 158–172, Jan. 2011.

[21] J. C. Vásquez, J. M. Guerrero, M. Savaghebi, J. Eloy-Garcia, and R. Teodorescu, "Modeling, analysis, and design of stationary-reference-frame droop-controlled parallel three-phase voltage source inverters," *IEEE Trans. Ind. Electron.*, vol. 60, no. 4, pp. 1271–1280, Apr. 2013.

[22] Q.-C. Zhong and T. Hornik, *Control of Power Inverters in Renewable Energy and Smart Grid Integration*, vol. 97. Hoboken, NJ, USA: Wiley, 2012.

[23] S. Yang, Q. Lei, F. Z. Peng, and Z. Qian, "A robust control scheme for grid-connected voltage-source inverters," *IEEE Trans. Ind. Electron.*, vol. 58, no. 1, pp. 202–212, Jan. 2011.

[24] S. A. Khajehoddin, M. Karimi-Ghartemani, P. K. Jain, and A. Bakhshai, "A control design approach for three-phase grid-connected renewable energy resources," *IEEE Trans. Sustain. Energy*, vol. 2, no. 4, pp. 423–432, Oct. 2011.

[25] M. A. Mahmud, H. R. Pota, and M. J. Hossain, "Nonlinear current control scheme for a single-phase grid-connected photovoltaic system," *IEEE Trans. Sustain. Energy*, vol. 5, no. 1, pp. 218–227, Jan. 2014.

[26] S. Dasgupta, S. N. Mohan, S. K. Sahoo, and S. K. Panda, "Lyapunov function-based current controller to control active and reactive power flow from a renewable energy source to a generalized three-phase microgrid system," *IEEE Trans. Ind. Electron.*, vol. 60, no. 2, pp. 799–813, Feb. 2013.

[27] J. Hu, L. Shang, Y. He, and Z. Q. Zhu, "Direct active and reactive power regulation of grid-connected DC/AC converters using sliding mode control approach," *IEEE Trans. Power Electron.*, vol. 26, no. 1, pp. 210–222, Jan. 2011.

[28] M. Benchagra, M. Hilal, Y. Errami, M. Maaroufi, and M. Ouassaid, "Nonlinear control of DC-bus voltage and power for voltage source inverter," in *Proc. IEEE Int. Conf. Multimedia Comput. Syst.*, May 2012, pp. 1049–1054.

[29] W. Li, X. Ruan, D. Pan, and X. Wang, "Full-feedforward schemes of grid voltages for a three-phase *LCL*-type grid-connected inverter," *IEEE Trans. Ind. Electron.*, vol. 60, no. 6, pp. 2237–2250, Jun. 2013.

[30] N. Mahdian-Dehkordi, M. Namvar, H. Karimi, P. Piya, and M. Karimi-Ghartemani, "Nonlinear adaptive control of grid-connected three-phase inverters for renewable energy applications," *Int. J. Control*, vol. 90, no. 1, pp. 53–67, 2017.

[31] T. K. Roy, M. A. Mahmud, A. M. T. Oo, R. Bansal, and M. E. Haque, "Nonlinear adaptive backstepping controller design for three-phase grid-connected solar photovoltaic systems," *Electr. Power Compon. Syst.*, vol. 45, no. 20, pp. 2275–2292, 2018.

[32] J.-J. E. Slotine *et al.*, *Applied Nonlinear Control*, vol. 199, no. 1. Englewood Cliffs, NJ, USA: Prentice-Hall, 1991.

[33] M. F. Heertjes and Y. Vardar, "Self-tuning in sliding mode control of high-precision motion systems," *IFAC Proc. Vol.*, vol. 46, no. 5, pp. 13–19, 2013.

[34] M. J. Santofimia, X. del Toro, P. Roncero-Sánchez, F. Moya, M. A. Martinez, and J. C. Lopez, "A qualitative agent-based approach to power quality monitoring and diagnosis," *Integr. Comput.-Aided Eng.*, vol. 17, no. 4, pp. 305–319, 2010.

AMMAR AHMAD received the B.Sc. degree in electrical engineering from the University of Engineering and Technology at Peshawar, Peshawar, Pakistan, in 2015, and the M.S. degree in electronic engineering from the GIK Institute of Engineering Sciences and Technology, Pakistan, in 2018. He joined Huawei Technologies, Pakistan, as a Project Supervisor. He is currently a Graduate Assistant with the GIK Institute of Engineering Sciences and Technology. His research interests include renewable energy systems, power electronics, and the robust control of nonlinear systems and flight control systems.

NASIM ULLAH received the Ph.D. degree in mechatronics engineering from Beihang University, Beijing, China, in 2013. From 2006 to 2010, he was a Senior Design Engineer with IICS, Pakistan. He is currently an Associate Professor with the Department of Electronics Engineering, University of Technology, Nowshehra, Pakistan. His research interests include renewable energy systems, energy conversion and conservation, microgrids, FACTS controllers, flight control systems, integer and fractional order modeling of dynamic systems, integer/fractional order adaptive robust control methods, fuzzy/NN, hydraulic and electrical servos, and epidemic and vaccination control strategies.

NISAR AHMED received the B.S. degree in electrical and electronics engineering from the University College of Engineering and Technology, Mirpur, Pakistan, in 1989, and the Ph.D. degree in control systems engineering and DIC electrical and electronic engineering from the Imperial College of Science, Technology and Medicine, London, U.K., in 1999. He joined the Water and Power Development Authority (WAPDA), Pakistan, as an Assistant Engineer, in 1990. In 1994, he was with WAPDA, where he participated in foreign training on 500-MW combined cycle power plant with Siemens, Germany. He is currently a Professor and the Dean of the Faculty of Electronic Engineering, GIK Institute of Engineering Sciences and Technology, Pakistan. His current research interests include Krylov subspace methods for model reduction of large-scale systems, renewable energy systems, and robust control system design for multivariable systems.

ASIER IBEAS was born in Bilbao, Spain, in 1977. He received the M.Sc. degree in applied physics and the Ph.D. degree in automatic control from the University of the Basque Country, Spain, in 2000 and 2006, respectively. He is currently an Associate Professor in control systems with the Autonomous University of Barcelona, Spain. He is also a Full Professor with the Catalan Agency for Quality in Higher Education. He has authored over 130 contributions in international journals and conferences. He has supervised and participated in numerous research projects funded by regional and national agencies. He is currently advising several doctoral thesis. His research interests include time-delayed systems, robust adaptive control, the applications of artificial intelligence to control systems design, and unconventional applications of control, such as to epidemic systems, supply chain management, and financial systems.

GHULAM MEHDI received the M.S. degree in electronic engineering from Linköping University, in 2007, and the Ph.D. degree in electronics engineering from Beihang University, Beijing China, in 2014. He is currently a Researcher with the Center of Excellence in Science and Applied Technology, Pakistan. His active research lines are RF electronics, radars, and signal processing.

JORGE HERRERA received the degree in electronic engineering from the University of Quindio, Colombia, in 2004, and the Ph.D. degree in industrial computing and advanced techniques of production from the Autonomous University of Barcelona, Spain, in 2011. He is currently a Full Professor with the Engineering Department, Universidad de Bogotá Jorge Tadeo Lozano, Bogotá, Colombia. He is also the Director of the Industrial Engineering Program and the Director of the master's degree in engineering management. His active research lines are parametric identification and adaptive control.

ANWAR ALI was born in Mardan, Pakistan, in 1981. He received the B.E. degree in electronics engineering from NED UET, Karachi, Pakistan, in 2004, and the M.S. degree in electronics engineering and the Ph.D. degree in electronics and communication engineering from the Polytechnic University of Turin, Italy, in 2010 and 2014, respectively. From 2014 to 2017, he was an Assistant Professor with the Electrical Engineering Department, Foundation for Advancement of Science and Technology, NUCES, Peshawar, Pakistan. Since 2017, he has been an Assistant Professor with the Electrical Engineering Technology Department, University of Technology, Nowshera, Pakistan. His research interests include the design and development of power management, attitude determination, and control subsystems of small satellites. He is currently involved in the areas of thermal analysis and thermal modeling of aerospace systems, power electronics applications, and renewable energy systems.